Biomolecular simulations of membranes: Physical properties from different force fields

Shirley W. I. Siu,[1] Robert Vácha,[2] Pavel Jungwirth,[2] and Rainer A. Böckmann[1,a)]
[1]*Theoretical and Computational Membrane Biology, Center for Bioinformatics, Saarland University, P.O. Box 151150, 66041 Saarbrücken, Germany*
[2]*Institute of Organic Chemistry and Biochemistry, Academy of Sciences of the Czech Republic, and Center for Biomolecules and Complex Molecular Systems, Flemingovo nám. 2, 16610 Prague 6, Czech Republic*

(Received 28 December 2007; accepted 22 February 2008; published online 27 March 2008)

Phospholipid force fields are of ample importance for the simulation of artificial bilayers, membranes, and also for the simulation of integral membrane proteins. Here, we compare the two most applied atomic force fields for phospholipids, the all-atom CHARMM27 and the united atom Berger force field, with a newly developed all-atom generalized AMBER force field (GAFF) for dioleoylphosphatidylcholine molecules. Only the latter displays the experimentally observed difference in the order of the C2 atom between the two acyl chains. The interfacial water dynamics is smoothly increased between the lipid carbonyl region and the bulk water phase for all force fields; however, the water order and with it the electrostatic potential across the bilayer showed distinct differences between the force fields. Both Berger and GAFF underestimate the lipid self-diffusion. GAFF offers a consistent force field for the atomic scale simulation of biomembranes. © *2008 American Institute of Physics*. [DOI: 10.1063/1.2897760]

I. INTRODUCTION

Membranes are an indispensable constituent of biological cells. Apart from their apparent role in compartmentalization, they provide a unique hydrophilic and hydrophobic platform for the adsorption or anchoring of proteins to the interface, or for transmembrane proteins interacting mainly with the hydrophobic core. Lipid bilayers provide a highly modulative environment interacting, presumably affecting, and possibly also keeping control of the function of, e.g., membrane ion channels and pores. The lipid-protein interaction is exerted both by hydrophobic interactions between the lipid acyl chains and the protein surface and by polar interactions at the lipid-water interface. Changes in the interaction profile may be attained by variations in the (local) membrane composition or that of the surrounding solvent or by changes in the temperature or pressure. Thereby, also the characteristic lateral pressure profile across the membrane is modified which may induce a shift of conformational equilibria between different states of membrane proteins, e.g., between the open and closed states of membrane channels.[1,2] Molecules strongly interacting with membranes are, e.g., cholesterol,[3,4] anesthetics,[5,6] and monovalent[7,8] and divalent cations.[9,10] The latter bind tightly to the carbonyl oxygens of phospholipids and thereby increase the lipid packing density as well as modify the lipid headgroup orientation.[8,10] Only recently, the importance of membrane thermodynamics for the understanding of propagating nerve pulses[11] or of the macroscopic effect of general anesthetic action[12] has been stressed.

Molecular dynamics (MD) simulation has been proven to be a powerful tool for the study of structural and dynamical properties of lipid membranes in atomic detail.[13–15] In recent years with the dramatic increase in computing power, membrane simulation has reached an unprecedented time scale, allowing the study of processes such as membrane assembly, fusion, domain formation, and protein/peptide/DNA interactions to be simulated while attaining statistical significance. In MD simulations, the intra- and intermolecular interactions of the lipids (also with the environment) are represented by specific potential functions (known as force fields). Parameters of the force fields are optimized empirically to reproduce both *ab initio* data and experimental observables. It was shown recently that—apart from appropriate simulation conditions—the quality of the force field is a crucial ingredient in obtaining reliable computational results in simulations of lipid bilayers.[16]

There are two most commonly used lipid force fields nowadays. The all-atom model CHARMM27,[17] evolved from the old CHARMM22,[18] was optimized on the condensed phase properties of alkanes. Similarly, the united-atom model of Berger *et al.*[19,20] (aliphatic hydrogen atoms implicitly treated), based on the united-atom version of Optimized Potential for Liquid Simulations (OPLS),[21] was parametrized against pentadecane. Both models have been extensively applied in a variety of membrane and membrane-protein studies and proved to show fairly agreeable results. Often, the Berger force field is preferred due to the greatly reduced computational cost with respect to all-atom lipid force fields.[22] Frequently, the united-atom force field for lipids is combined with the all-atom OPLS (Ref. 23) force field for the simulation of protein-membrane systems instead of the more consistent CHARMM force field for both lipids and proteins. The combination of different force fields, however, is

a)Electronic mail: rainer@bioinformatik.uni-saarland.de.

not straightforward and requires careful investigation.[22]

The main focus in parametrizations and tests of the lipid force field is typically on the reproduction of experimentally accessible lipid bilayer properties such as the electron density profile, the area per lipid, the lipid order parameters, and the thickness of the membrane. These are generally well reproduced, with a few exceptions like the measured difference in the order parameters of the C2 atoms between the two acyl chains (typically similar in the force fields) or a too low lipid headgroup hydration at low water content.[16] Also, protein-lipid interactions in combined Berger/GROMOS or Berger/OPLS lipid-protein simulations are possibly overestimated, resulting in drastic changes of lipid properties upon insertion of proteins.[22,24] This is a consequence of the lack of experimental data on protein-lipid interactions to be used in parametrizations.

Deviations from experiment were also observed for the partitioning of anesthetics in lipid membranes: MD simulations of the spontaneous insertion of 1-alkanols of varying chain lengths into phosphatidylcholine bilayers applying the united-atom Berger force field for the lipids and the GROMOS force field for the 1-alkanols resulted in satisfying partition coefficients for the long-chain 1-alkanols.[25] However, for ethanol the partition coefficient was increased by a factor of 7–200 with respect to experiment, depending on the force field chosen for ethanol.[25,26] Similar large ethanol partition coefficients were also obtained by consistently applying the CHARMM27 all-atom force field.[27]

Recently, the general all-atom AMBER force field (GAFF) was developed.[28] In contrast to CHARMM and the previous version of AMBER, it is designed to be a general purpose force field, allowing extension to arbitrary organic molecules while keeping consistency with the parameters and forms of the existing force field. In principle, GAFF can also be used in membrane simulations, and in fact, Jójárt and Martinek[29] reported a tens of nanosecond test on GAFF in palmitoyoleoylphosphatidylcholine (POPC) lipid bilayer simulations in various ensembles, which showed its potency in good agreement with experimental values. Thus, GAFF is expected to open the lane toward a consistent all-atom force field for proteins, lipids, and other arbitrary organic molecules.

Here, we developed the all-atom GAFF for dioleoylphosphatidylcholine (DOPC) combined with and restrained electrostatic potential[30,31] (RESP) atomic partial charges. In a first step, structural and dynamical properties of a fully hydrated DOPC bilayer were compared to those obtained applying the united-atom force field of Berger *et al.* and with the all-atom CHARMM27 force field. Besides the structural and dynamical properties of the lipid bilayer, special emphasis was put on water properties close to the lipid-water interface and the resulting electrostatic potential across the phospholipid bilayer. Despite overall agreement in the reproduction of coarse properties of lipid bilayers, the force fields showed distinct differences in the phospholipid headgroup orientation, the water content of the interfacial region, the orientation of the carbonyl group, and the order of the two acyl chains. For the latter, only GAFF reflected the experimentally found order asymmetry at the beginning of the chains.

II. METHODS

A. Initial structures

Two different systems of DOPC bilayers were set up for this study: A full-atomistic model (with 72 DOPC lipids) for use with the general AMBER (GAFF) (Ref. 28) and the CHARMM force fields,[17] and a united-atom model (128 DOPC lipids) for use with the Berger force field.[19,20]

A full-atomistic, pre-equilibrated DOPC bilayer[32] (1500 ps snapshot, available from Ref. 33) was taken as the starting structure. It consists of 72 lipids at low hydration with only five to six water molecules per lipid. To ensure full hydration, the simulation box was enlarged, and additional water molecules were added to the water phase to attain a water to lipid ratio of 37.9 [above the suggested experimental value of 32.5 (Ref. 34)]. In total, the simulation system contained 2727 water molecules, forming a water slab of about 1.8 nm thickness. The simulation system consists of 18 117 atoms.

The united-atom model was created from a pre-equilibrated POPC membrane model of 128 lipids (100 ns) used in our previous study.[8] To convert to the DOPC model, two additional–CH_2–groups were added to the palmitoyl chain of each POPC lipid in a *trans* configuration. Additionally, the single bond between carbon atoms 9 and 10 was changed to be double bonded. The number of water molecules was 4798, resulting in a water to lipid ratio of 37.4. The total system size was 21 279 atoms.

B. Force field parameters

Three popular force fields were chosen in this study. The lipid parameters for the united-atom model of DOPC were based on Berger. Parameters for the unsaturated carbons, however, were taken from the GROMOS87 force field.[35] The CHARMM27 force field for DOPC was converted to GROMACS topology (conversion script kindly provided by Mark Abraham). Note that the conversion is not exact and dihedrals were fitted to Ryckaert–Bellemans dihedrals to reproduce the CHARMM27 (Ref. 17) force field the best.

For GAFF, the atomic charges for the lipids were evaluated using antechamber with the RESP potential fit method[30,31] after an *ab initio* HF/6-31G* calculation using the GAUSSIAN03 program package[36] and fitting the electrostatic potential at points selected according to the Merz–Singh–Kollman scheme. The RESP fitted charges from 72 lipid conformations taken from the Feller model were averaged and rounded to two decimal points. The rounding was done with preference to conserve the total charge on a chemical group.

As shown in Table I (also see Fig. 1 for the naming convention of atoms), the total charges on the choline and phosphate groups, on the glycerol backbone, on the carbonyl groups, and the acyl chains are similar for all investigated force fields. Differences are especially seen in the charge distribution of the choline group: The nitrogen atom is almost uncharged in GAFF but highly negatively charged in the CHARMM27 and in the Berger force field. The acyl chain atoms are neutral in the Berger force field; for GAFF only the beginning of the chain (C2 atom), the unsaturated car-

TABLE I. The atom types and the partial charges of all atoms used in the respective force fields.

	GAFF		CHARMM27		Berger	
Name	Type	Charge	Type	Charge	Type	Charge
Choline	Σ	1.1	Σ	1.1	Σ	1.4
N1	n4	0.02	NTL	−0.60	LNL	−0.50
C2	c3	−0.12	CTL5	−0.35	LC3	0.40
H2a/b/c	hx	0.11	HL	0.25		
C3	c3	−0.12	CTL5	−0.35	LC3	0.40
H3a/b/c	hx	0.11	HL	0.25		
C4	c3	−0.12	CTL5	−0.35	LC3	0.40
H4a/b/c	hx	0.11	HL	0.25		
C5	c3	−0.01	CTL2	−0.10	LH2	0.30
H5a/b	hx	0.09	HL	0.25		
C6	c3	0.16	CTL2	−0.08	LC2	0.40
H6a/b	h1	0.06	HAL2	0.09		
Phosphate	Σ	−1.28	Σ	−1.2	Σ	−1.4
O7	os	−0.42	OSL	−0.57	LOS	−0.80
P8	p5	1.12	PL	1.5	LP	1.70
O9	o	−0.78	O2L	−0.78	LOM	−0.80
O10	o	−0.78	O2L	−0.78	LOM	−0.80
O11	os	−0.42	OSL	−0.57	LOS	−0.70
Glycerol	Σ	−0.1	Σ	−0.32	Σ	−0.2
C12	c3	0.06	CTL2	−0.08	LC2	0.40
H12a	h1	0.08	HAL2	0.09		
H12b	h1	0.08	HAL2	0.09		
C13	c3	0.14	CTL1	0.04	LH1	0.30
H13	h1	0.13	HAL1	0.09		
C14	c3	0.01	CTL2	−0.05	LC2	0.50
H14a	h1	0.10	HAL2	0.09		
H14b	h1	0.10	HAL2	0.09		
O15	os	−0.40	OSL	−0.34	LOS	−0.70
O16	os	−0.40	OSL	−0.34	LOS	−0.70
Carbonyl	Σ	0.28	Σ	0.22	Σ	0.2
C1a	c	0.71	CL	0.63	LC	0.80
O1a	o	−0.57	OBL	−0.52	LO	−0.60
C1b	c	0.71	CL	0.63	LC	0.70
O1b	o	−0.57	OBL	−0.52	LO	−0.70
Acyl chain	Σ	0.0	Σ	0.1	Σ	0.0
C2	c3	−0.12	CTL2	−0.08	LP2	0.000
H2a/b	hc	0.05	HAL2	0.09		
C3	c3	−0.02	CTL2	−0.18	LP2	0.000
H3a/b	hc	0.02	HAL2	0.09		
C4	c3	−0.03	CTL2	−0.18	LP2	0.000
H4a/b	hc	0.02	HAL2	0.09		
C5	c3	−0.02	CTL2	−0.18	LP2	0.000
H5a/b	hc	0.01	HAL2	0.09		
C6	c3	−0.02	CTL2	−0.18	LP2	0.000
H6a/b	hc	0.01	HAL2	0.09		
C7	c3	−0.02	CTL2	−0.18	LP2	0.000
H7a/b	hc	0.02	HAL2	0.09		
C8	c3	0.04	CTL2	−0.18	LP2	0.000
H8a/b	hc	0.03	HAL2	0.09		
C9	c2	−0.25	CEL1	−0.15	LH1	0.000
H9	ha	0.13	HEL1	0.15		
C10	c2	−0.24	CEL1	−0.15	LH1	0.000
H10	ha	0.13	HEL1	0.15		
C11	c3	0.02	CTL2	−0.18	LP2	0.000
H11a/b	hc	0.03	HAL2	0.09		
C12	c3	−0.01	CTL2	−0.18	LP2	0.000
H12a/b	hc	0.01	HAL2	0.09		
C13	c3	−0.00	CTL2	−0.18	LP2	0.000
H13a/b	hc	0.00	HAL2	0.09		
C14	c3	−0.00	CTL2	−0.18	LP2	0.000
H14a/b	hc	0.00	HAL2	0.09		
C15	c3	−0.02	CTL2	−0.18	LP2	0.000
H15a/b	hc	0.01	HAL2	0.09		
C16	c3	−0.01	CTL2	−0.18	LP2	0.000
H16a/b	hc	0.01	HAL2	0.09		
C17	c3	0.02	CTL2	−0.18	LP2	0.000
H17a/b	hc	0.01	HAL2	0.09		
C18	c3	−0.13	CTL3	−0.27	LP3	0.000
Ha/b/c	hc	0.03	HAL3	0.09		

bons and the attached hydrogens, as well as the terminal methyl groups carry charges significantly different from 0. In contrast, all atoms of the acyl chains have non-negligible charges in the CHARMM27 force field.

For the DOPC bilayer simulation applying the Berger force field the Simple Point Charge (SPC) water model[37] was chosen as this force field was developed with SPC water. For

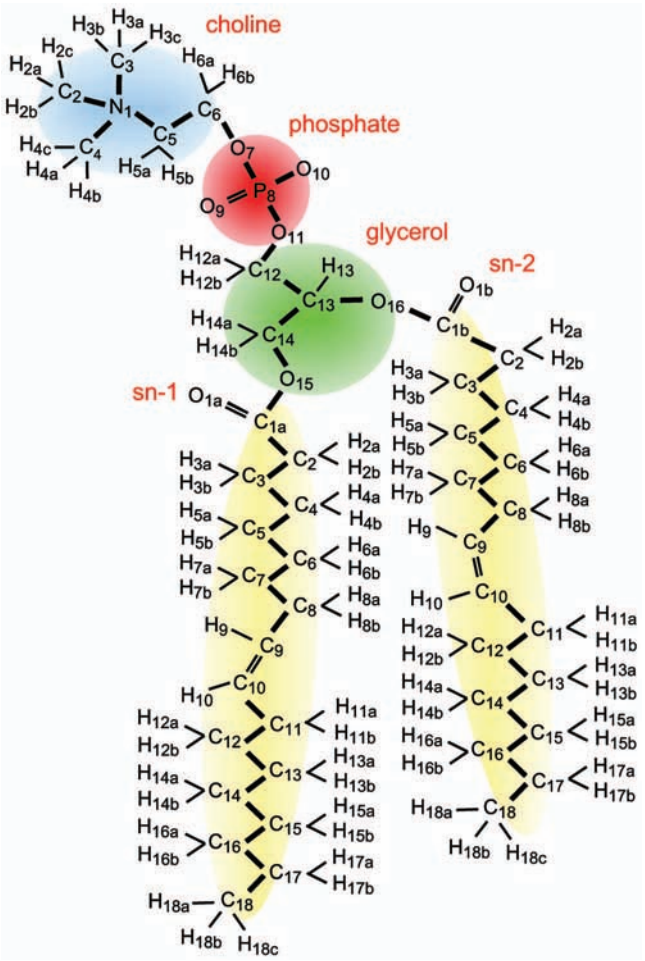

FIG. 1. (Color) Schematic drawing of the DOPC lipid and the naming convention used in this manuscript.

TABLE II. Overview of the simulation systems presented in this study.

System	No. of lipid	No. of water	Lipid force field	Water model	Ensemble
A	72	2727	GAFF all-atom	SPC/E	*NPT*
B	72	2727	GAFF all-atom	SPC/E	$NP\gamma T$
C	72	2727	GAFF all-atom	TIP3P	$NP\gamma T$
D	72	2727	CHARMM all-atom	TIP3P	$NP\gamma T$
E	128	4789	Berger united-atom	SPC	*NPT*

the same reason, the bilayer applying the CHARMM27 lipid force field was solvated with TIP3P water.[38] For the newly developed GAFF, both the Extended Simple Point (SPC/E) (Ref. 39) water model and the TIP3P water model (starting from a snapshot of the SPC/E system after 100 ns) were chosen for comparison.

C. Simulation conditions

All simulations were performed using the GROMACS package.[40,41] Periodic boundary conditions were applied in all directions. The system was separately coupled to a temperature bath at 310 K for the lipids and the water molecules with a coupling time constant of 0.1 ps^{-1}.[42] Bonds to H atoms were constrained using the LINCS (Ref. 43) and the SETTLE algorithms.[44] This allowed for an integration step size of 2 fs. The nonbonded pair list was updated every ten steps with a cutoff of 1.0 nm. For the short range van der Waals interactions, a cutoff distance of 1.0 nm was used. In treating the long-range electrostatics, the particle-mesh ewald method with a grid spacing of 0.12 nm and cubic interpolation was adopted.

Two systems were simulated at constant pressure (GAFF all-atom and Berger united-atom, systems A and E in Table II), applying a semi-isotropic pressure coupling with a barostat relaxation time of 1 ps at a pressure of 1 bar.[42] In order to ensure an area per lipid in agreement with experiment, DOPC bilayers simulated applying all-atom force fields were additionally subjected to a surface tension γ (γ =22 dyn/cm per surface; systems B, C, and D). In the following, constant temperature and pressure conditions will be termed NPT ensembles, simulation conditions including surface tension $NP_\gamma T$ ensembles. However, note that the Berendsen thermostat and barostat do not strictly provide a correct *NPT* ensemble. The volume compressibility was chosen to be 4.5×10^{-5} bar^{-1}. Data were collected every picosecond.

All simulation systems were energy minimized with the steepest descent method and subsequently simulated for 100 ns each. For the analyses, the first 20 ns were disregarded due to equilibration effects.

Table II gives a summary of the simulation systems presented in this manuscript. With a combination of different force fields, pressure coupling methods, and water models, a total of five systems were studied and compared.

D. Analysis

1. Lipid order parameter

The lipid order parameter, S_{CD}, is a direct measurement of the acyl chain order or disorder from the quadrupolar splitting in the NMR experiment. For the simulations, the molecular order parameter is given by[13]

$$S_{ij} = \tfrac{1}{2}\langle 3\cos\theta_i\cos\theta_j - \delta_{ij}\rangle, \tag{1}$$

where θ_i is the angle between the ith molecular axis ($i,j=x,y,z$) and the bilayer normal. When the C_nH bond vector is used as the molecular axis (say, z), then S_{zz} gives the experimentally measured S_{CD} value.[45] For the united-atom model which contains no explicit hydrogen atoms in the carbon tails, the segmental vector C_{n-1} to C_{n+1} is taken as the molecular axis of the C_n methylene group, about which the segment motion is assumed to be axially symmetric. Then, the deuterium order parameter S_{CD} is approximated by the following relations for saturated and unsaturated carbon tail atoms:[46]

$$-S_{CD}^{sat} = \tfrac{2}{3}S_{xx} + \tfrac{1}{3}S_{yy} \tag{2}$$

and

$$-S_{CD}^{unsat} = \frac{1}{4}S_{zz} + \frac{3}{4}S_{yy} \mp \frac{\sqrt{3}}{2}S_{yz}. \tag{3}$$

2. Lipid and water diffusion

The self-diffusion coefficient D of molecules can be calculated from the Einstein relation on Brownian motion:

$$2d_fD = \lim_{t\to\infty}\frac{1}{t}\langle (r(t)-r(0))^2\rangle, \tag{4}$$

where d_f is the number of translational degrees of freedom (for lateral diffusion $d_f=2$) and $r(t)$ is the position of the molecule at time t. In practice, the lateral self-diffusion coefficient is estimated from the slope of the molecule's mean square displacements (msds) d^2 [e.g., taken on the center of mass (c.m.) coordinates] in a defined time window averaged over all molecules N:[8]

$$d^2(t) = \frac{1}{N}\frac{\Delta t}{T-t}\sum_{i=1}^{N}\sum_{t_0=0}^{T-t-1}|r(t_0)-r(t_0+t)|^2. \tag{5}$$

The first sum runs over the N molecules and the second sum runs over all time frames smaller than $T-t$, where T is the sampling time (Δt is the time between two subsequent conformations).

For the lipids, the lateral msds were corrected for the c.m. motion of the respective monolayer.[8] c.m. removal allows a correction for correlated unidirectional motions. For the investigated system sizes the c.m. removal likely yields a too small value for the lipid diffusion.[47] However, without c.m. removal the diffusion coefficient might be severely overestimated due to correlations even with the second lipid

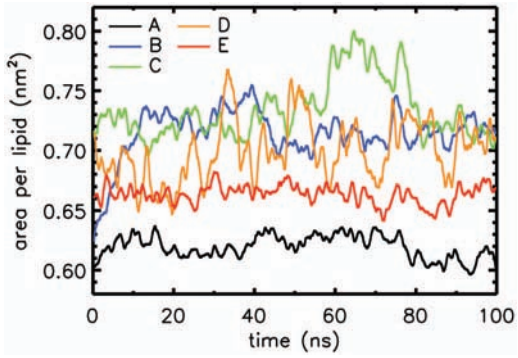

FIG. 2. (Color) Area per lipid for the five investigated systems in 100 ns simulation time smoothed by a sliding window of 1 ns length. Larger fluctuations were observed for systems applying surface tension (B, C, and D) as compared to those using semi-isotropic pressure coupling (A and E). Note that the experimental area per lipid for DOPC was measured to be 0.721 nm^2 at 30 °C (Ref. 79).

shell around a molecule: Transitions will propagate over distances larger than the box size[47] (for the 72 lipid system).

The errors were estimated by splitting the trajectories into pieces of 20 ns length (block averaging).

To obtain a spatially resolved water diffusion coefficient, the simulation box was divided into 40 slabs (i.e., ≈2 Å per slab) and the lateral diffusion in each slab was calculated by considering only the water molecules located in the same slab at time t_0 and at time t_0+t. Block averaging from 5 ns pieces of the production trajectory was used to obtain the mean and standard error of the coefficients.

For comparison, additional simulations of pure water boxes (containing 2182 water molecules, 5 ns simulation length each) yielded bulk water diffusion coefficients for the investigated water models.

3. Electrostatic potential

The electrostatic potential across the phospholipid bilayer was calculated by double integration of the averaged charge density ρ across the bilayer,

$$\phi(z) - \phi(z_0) = -\frac{1}{\epsilon_0}\int_{z_0}^{z} dz' \int_{z_0}^{z'} \rho(z'')dz''. \quad (6)$$

III. RESULTS

A. Area per lipid

The area per lipid is frequently used as a measure for the equilibration of the lipid bilayer system or to monitor phase transitions. In practice, the area per lipid is obtained as the lateral area of the simulation box (the *xy*-plane) divided by the number of lipids in one monolayer.

In Fig. 2, the area per lipid for the 100 ns trajectory of each simulation system is presented. Equilibration in the area per lipid is reached after approximately 20 ns for each system, and the analyses were conducted on the final 80 ns of the trajectories.

For a DOPC simulation applying the CHARMM27 force field without surface tension (data not shown) the area per lipid decreased to 0.56 nm^2 within 16 ns. This transition to a gel-like state was previously observed for a dipalmitoylphosphatidylcholine (DPPC) bilayer applying the same force field in the *NPT* ensemble.[48,49] Also, in a comparative simulation study of a DOPC bilayer at low hydration between the CHARMM and Berger force field in the *NPT* ensemble, a too small area per lipid was reported for the CHARMM27 force field.[50] The transition to a gel-like state can be prevented by application of a surface tension γ=22 dyn/cm (system D). Also for GAFF in the *NPT* ensemble the area per lipid was well below the crystallographic value (0.62 nm^2 versus 0.72 nm^2). Test simulations showed the best agreement to experimental data in the $NP_\gamma T$ ensemble by applying the same surface tension γ as for the CHARMM27 system (tested values γ=22,30,35 dyn/cm).

TABLE III. Averages and errors of the membrane structural parameters calculated by block averaging (block length of 20 ns). The membrane thickness was measured as the distance between the two peaks in the system electron density profiles. Errors in the area per lipid for systems D and E were rounded to 0.01 nm^2.

System	Area per lipid (nm^2)	Membrane thickness (nm)
Expt.[a]	0.721	3.71
A	0.62 ± 0.01	4.00 ± 0.05
B	0.72 ± 0.01	3.61 ± 0.04
C	0.74 ± 0.03	3.51 ± 0.13
D	0.71 ± 0.01	3.63 ± 0.13
E	0.66 ± 0.01	3.72 ± 0.11

[a]The experimental values were measured by Liu and Nagle (Ref. 79) using fully hydrated DOPC bilayers at 30 °C.

Table III shows that the area per lipid favorably agrees with the experimental value of 72 $Å^2$ for the GAFF and CHARMM27 systems (B, C, and D). However, lipids simulated in the Berger force field (*NPT*, system E) were too densely packed (area per lipid 8% below experiment).

B. Lipid headgroup orientation

Differences among the force fields in the lipid headgroup region are reflected, e.g., in the headgroup tilt with respect to the bilayer normal. The headgroup tilt was taken as the angle between the vector connecting the phosphorus and the nitrogen atoms and the bilayer normal. The most probable orientations as well as the width of the distribution of tilt angles are summarized in Table IV. The largest lipid headgroup tilt angles were observed for the Berger force field (86°, system E) and the smallest for GAFF (59° for system A and 67° for system B). The distribution of tilt angles is broad for all investigated force fields, with a width at half maximum from 62° (CHARMM27) to 88° (Berger). The difference in the lipid headgroup tilt is also reflected in the electron density profiles across the bilayer (see below). The straightened headgroup orientation in the CHARMM27 force field and in GAFF enabled an increased water content in the interfacial membrane-water region.

C. Lipid order parameter

The ensemble averaged deuterium lipid order parameters $|S_{CD}|$ of the two carbon tails are separately shown in Fig. 3.

TABLE IV. Distribution of lipid headgroup orientations computed as the angle between the vector connecting the phosphorus and the nitrogen atoms and the bilayer normal. Both the maximum of the distribution—the most probable orientation—and its width are given. The last two columns give the most probable total dipole moment of the individual lipids in the respective force fields (± the width of a fitted Gaussian distribution) as well as the average of the dipole moment along the bilayer normal (z-direction).

System	Most probable orientation (deg)	Width at half maximum (deg)	$M \pm \sigma$ (D)	M_z (D)
A	59	79 $(^{+46}_{-33})$	23.2 ± 3.8	4.3
B	67	74 $(^{+36}_{-38})$	23.2 ± 2.8	4.0
C	69	82 $(^{+39}_{-43})$	23.3 ± 2.7	3.5
D	73	62 $(^{+32}_{-30})$	23.7 ± 3.2	2.1
E	86	88 $(^{+32}_{-56})$	27.1 ± 3.8	8.1

All systems displayed the general trend of decreasing order along the chain toward the core of the bilayer with a prominent dip close to or at the double-bond segment (carbon atoms 9 and 10). Similar characteristics were observed for the oleoyl chain of POPC by deuterium NMR (Ref. 51) and in MD simulations (see, e.g., the recent work by Pandit *et al.*,[52] and on DOPC by the DROSS NMR technique.[53] Both ^{2}H-NMR and ^{2}H-^{13}C DROSS NMR found the dip located at the C10 atom.

In the MD simulations, however, the position of the central discontinuity differed among the investigated force fields: It occurred in both chains at C9 for CHARMM27 (D), and at C10 for Berger (E), while for GAFF (B) the dip is seen at C11 for the *sn*-1 chain and at C10/C11 for the *sn*-2 chain (see Fig. 1 for the naming). Atoms more far away from the glycerol backbone (C12—C18) showed the same order for both chains in all force fields, which is in agreement with NMR data. This finding was even observed for the saturated and unsaturated chains of POPC.[51]

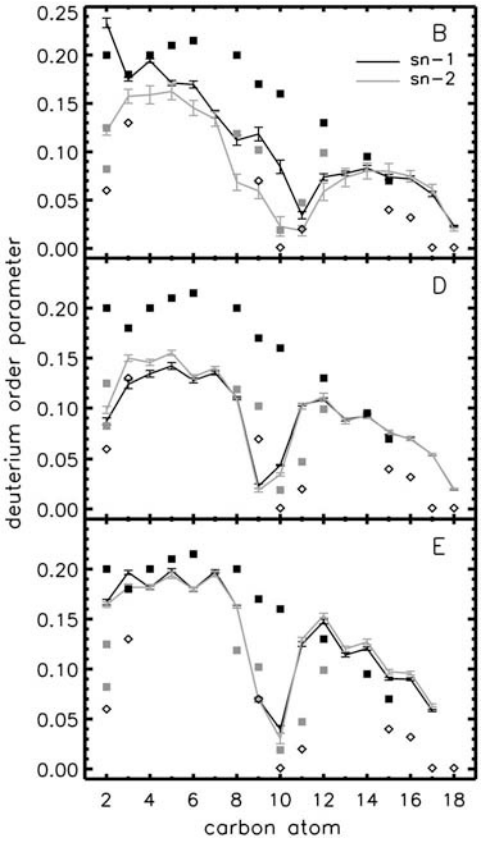

FIG. 3. Deuterium order parameters, $|S_{CD}|$, for the two acyl chains of DOPC lipids analyzed for systems B, D, and E. Error bars indicate the errors of the means from block averaging (blocks of 20 ns length). Experimental values are given for the POPC *sn*-1 (*black squares*) and *sn*-2 chain (*gray squares*) at 27 °C (Ref. 51), and for DOPC *sn*-2 at 37 °C (Ref. 53) (◇ symbols). Note that the double-bonded carbon atoms are at positions 9 and 10.

In contrast, deuterium NMR revealed differences close to the glycerol backbone even for identical chains: In studies on DPPC (Ref. 54) and POPC (Ref. 51) a distinctly smaller order was observed for the C2 atom of the *sn*-2 acyl chain as compared to the *sn*-1 chain. This inequivalence of the chains close to the glycerol backbone was found to be independent of the polar headgroup and thus to be a general feature of phospholipids within membranes.[51] From NMR results it was concluded that the orientations in the beginning of the chains differ significantly with chain 1 being oriented perpendicular and chain 2 parallel to the bilayer surface.[54] The suggestion of different conformations of the beginnings of the two chains was supported by x-ray diffraction studies.[55] Only the new GAFF for DOPC reflected the general order characteristics with a significantly enhanced order for the C2 atom of the *sn*-1 chain. The Berger and CHARMM27 force fields show similar profiles for both chains close to the glycerol backbone as was also observed in earlier studies based on multinanosecond simulations.[7,25,56] For DPPC, the C2 order for the *sn*-1 chain was even reported to be smaller than that of the *sn*-2 chain applying the CHARMM27 force field.[17] A previous study on DOPC (Ref. 57) applying a modified GROMOS96 force field[58] reported tiny differences for the C2 order parameters between the chains, together with the dip located at the C9 (Ref. 57) atom similar to the CHARMM27 force field or at the C10 atom.[58]

The conformation in the beginning of the acyl chain is described by the orientation of the vector connecting the C1 and the C2 atom: For both CHARMM27 and GAFF lipids, chain 1 is oriented perpendicular to the bilayer surface (maximum of the probability distribution of angles to bilayer normal ≈180°, data not shown). While the distribution is only slightly shifted to smaller angles for chain 2 in CHARMM27 (163°, width 44°), the second chain adopts a significantly different orientation with respect to chain 1 in GAFF (133°, width 27°). Like for CHARMM27, the orientations of the C1—C2 vector for the Berger force field are similar to 160° and 144° for the two chains.

In the deuterium NMR experiment,[51] two signals were observed at C2 indicating a nonequivalence of the two hydrogen positions only in this segment, due to different average orientations.[59] For the all-atom GAFF and CHARMM systems, the order parameter of each individual C—H bond can separately be determined. In the simulations (data not shown) the order of the two hydrogens is very similar in all methylene segments including the C2 segment. The difference of the mean between the two hydrogens in C2 is only 0.01 for GAFF and is 0.02 for CHARMM, while the experimental difference is about 0.05. Hence, the nonequivalent feature at C2 cannot be reproduced by any of the tested force fields.

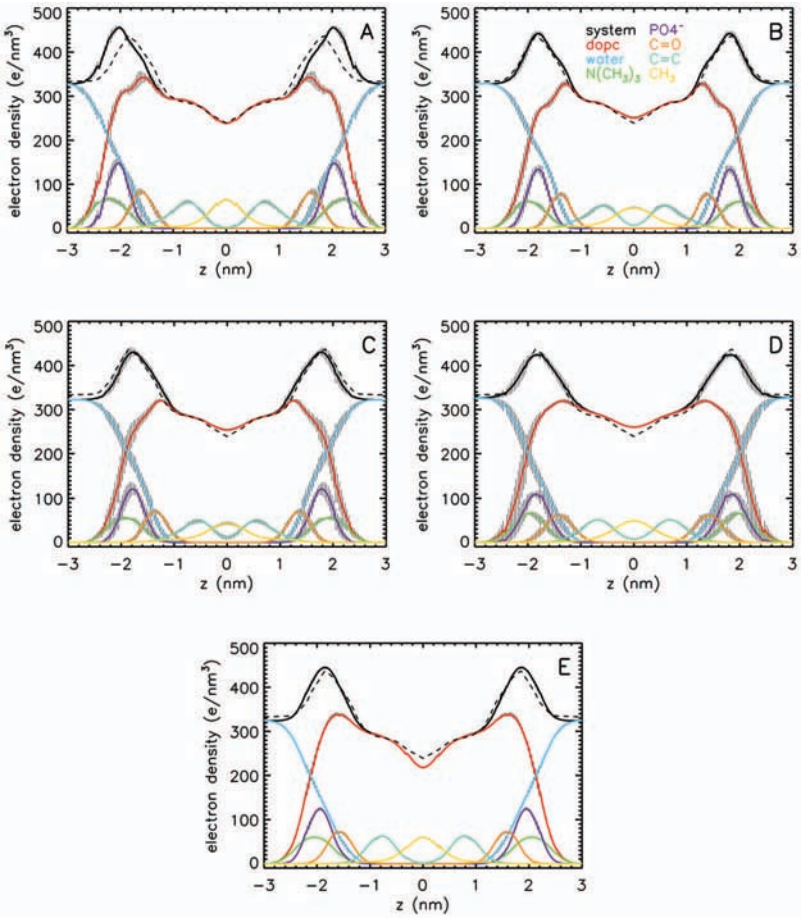

FIG. 4. (Color) The (symmetrized) electron density profiles of the overall and individual chemical components of all simulation systems. The profiles are centered at the core of the bilayer, and the standard errors (as shown here in *gray* lines) are calculated by dividing the trajectories into blocks of 20 ns length. The profile was computed by placing the appropriate number of electrons at the center of atomic nuclei binning along the direction of the membrane normal (bin width of 0.3 Å). The experimental density profile (Ref. 79) is shown as a *dashed* line.

D. Density profile and membrane thickness

Electron density profiles of the simulated membrane systems can directly be compared to x-ray experimental data. Figure 4 shows the overall electron density and the electron densities of individual chemical groups of the bilayer.

The total electron density of the GAFF system without surface tension (A) shows good agreement with the x-ray data in the hydrophobic core region. However, the membrane thickness measured as the distance between the maxima of the electron density profiles is increased by ≈3 Å with respect to experiment (see Table III). The GAFF-SPC/E system applying surface tension (B) revealed overall excellent agreement with the experimental profile. Using the TIP3P instead of the SPC/E water model together with GAFF (C) resulted in a decreased density at the membrane-water interface.

Also the electron density profile obtained for the CHARMM27 system (D) agrees well with the experimental profile, except for the region of the central methyl groups for which the density is significantly enhanced with respect to experiment. Interestingly, systems with the TIP3P water model showed enhanced bilayer fluctuations, resulting in increased error bars for the membrane thickness (Table III).

Although the membrane thickness is best modeled by the Berger force field (E), the electron density profile is at variance with the x-ray data. The headgroup region is broadened, and the methyl group region is underestimated.

For comparison between the investigated force fields, Fig. 5 shows a close-up view of the membrane-water interface for the GAFF-SPC/E, CHARMM27-TIP3P, and Berger-SPC force field combinations. Although the membrane thickness is similar for all three force fields, both GAFF and

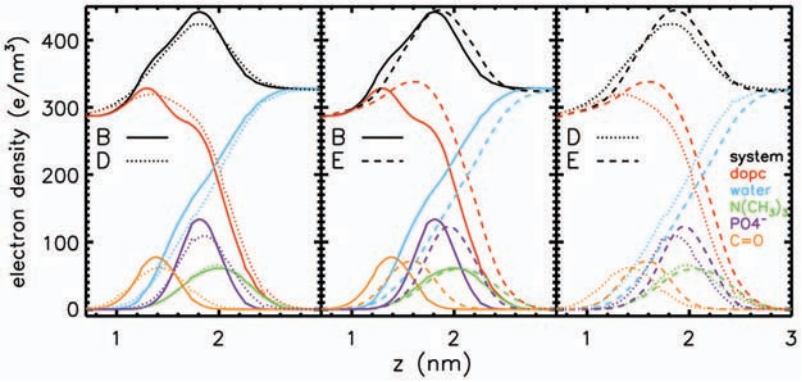

FIG. 5. (Color) Comparison of the electron density profiles at the membrane-water interface (centered on the lipid bilayer) for force field combinations GAFF-SPC/E, CHARMM27-TIP3P, and Berger-SPC (systems B, D, and E). The same coloring scheme for Fig. 4 is used here.

CHARMM27 show a drastically increased water content (*blue* lines) in the lipid headgroup region as compared to Berger (with root mean square deviations, rms, of 37 and 27 e/nm^3, respectively), coupled to a decreased DOPC electron density (red lines, with rms of 31 and 20 e/nm^3, respectively). While the membrane thickness between Berger and the all atom systems differs only by 1 Å, the carbonyl groups are shifted for Berger-SPC by ≈2 Å toward the headgroup region. The hydration of the carbonyl oxygens is significantly lowered for Berger lipids with respect to CHARMM27 and GAFF: The cumulative radial distribution yielded an average of only 1.5 water molecules around both carbonyl oxygens for Berger (taken at the first minimum of the radial distribution function, 0.55 for the *sn*-1 chain), but 3.4 (1.7) and 2.9 (1.4) water molecules for CHARMM27 and GAFF lipids, respectively.

E. Lipid and water diffusion

Lipids in the liquid crystalline phase diffuse in the plane of the bilayer due to thermal agitation. This diffusive movement can roughly be classified into two regimes: Fast fluctuation of the lipid in the local solvation cage[60] and a relatively slow but long distance diffusion in the bilayer. Different experimental methods acting on different time scales therefore obtain lipid diffusion coefficients differing by two to three orders of magnitude.

As shown in Fig. 6 (upper panel) the lipid msd for all systems clearly showed the existence of both long-range and short-range diffusion behaviors of lipids, with a smooth transition between the two regions. In order to determine the linear segment in the msd curve (long-range diffusion), the diffusion coefficient D was calculated using different time windows for the linear fit.

The values for D (Fig. 6, lower panel) converged between 3 ns (for systems A, B, and E) and 5 ns (C and D). Therefore, the diffusion coefficients for long-range lipid diffusion were consistently computed from a linear fit to the msd between 5 and 10 ns. The data are summarized in Table V. With the exception of the bilayer simulated applying the CHARMM27 force field (system D), all computed diffusion coefficients are smaller by a factor of 2–8 as compared to the experimental value of $D=13.7\times10^{-8}$ cm^2 s^{-1} [NMR on oriented bilayers at 308 K (Ref. 61)]. Interestingly, the DOPC diffusion is also strongly dependent on the force field used for the water molecules: While GAFF combined with SPC/E water yields a lipid diffusion coefficient of $D=(3.1\pm0.9)\times10^{-8}$ cm^2 s^{-1}, the diffusion is almost enhanced by a factor of 2 for GAFF combined with TIP3P water. Thus the increased bulk water diffusion of TIP3P with respect to SPC/E (see below) has also a pronounced influence on the lipids in a bilayer. Although the area per lipid is similar for both systems, the long-range lipid diffusion is about two times larger for the CHARMM27-TIP3P system as compared to GAFF-TIP3P. The CHARMM27 diffusion coefficient is, however, subject to a large error.

The diffusion coefficients obtained on the subnanosecond time scale decayed exponentially with increasing time scale. Values for the diffusion coefficient range between 5 $\times10^{-8}$ and 82×10^{-8} cm^2 s^{-1}, depending on the time scale and on the applied force field, and are in agreement with experimental diffusion coefficients obtained for DPPC of $(10-100)\times10^{-8}$ cm^2 s^{-1}.[60,62,63]

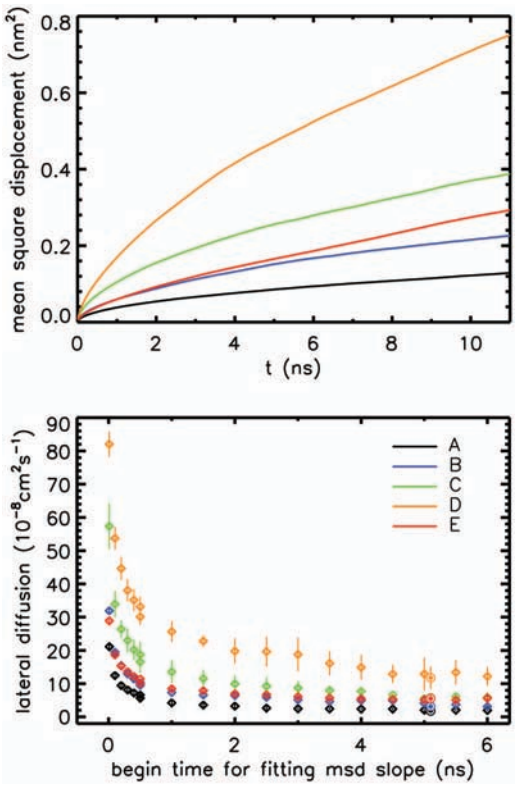

FIG. 6. (Color) Lipid diffusion coefficients calculated for different time lengths of the simulations by block averaging: The trajectory was divided into 20 ns pieces and the msd (upper panel) was calculated separately for each block. Diffusion coefficients (lower panel) computed for different time ranges were obtained by fitting different time windows of the msd curve. For the short-range diffusion (colored ◇ symbols), shorter time windows of 100 ps (fit starts between 10 and 500 ps) and 500 ps (fit starts between 500 ps and 6 ns) were used. For the long-range diffusion (colored ⊙ symbols) fitting was done on the linear segment of the msd curve between 5 and 10 ns.

The (lateral) water diffusion close to the phospholipid bilayer and in the interfacial region strongly depends on the water model applied in the simulation (see Fig. 7). While SPC/E water in GAFF simulations was largely immobilized

TABLE V. The calculated mean lateral diffusion coefficient for water molecules and for DOPC molecules. For water diffusion, the average was calculated from all water molecules in the system regardless of the distance to bilayer. For lipid diffusion, the long-range diffusion coefficients are shown here while the short-range diffusions are depicted in Fig. 6.

System	Water diffusion ($\times10^{-5}$ cm^2 s^{-1})	Lipid diffusion ($\times10^{-8}$ cm^2 s^{-1})
Expt.		13.7[a]
A	2.27 ± 0.03	1.79 ± 0.51
B	2.07 ± 0.03	3.13 ± 0.94
C	4.31 ± 0.08	5.71 ± 1.06
D	4.60 ± 0.08	11.76 ± 3.39
E	3.63 ± 0.02	5.52 ± 1.00

[a]The experimental lipid diffusion coefficient is taken from pulsed field gradient NMR experiments on oriented bilayers at 308 K (Ref. 61).

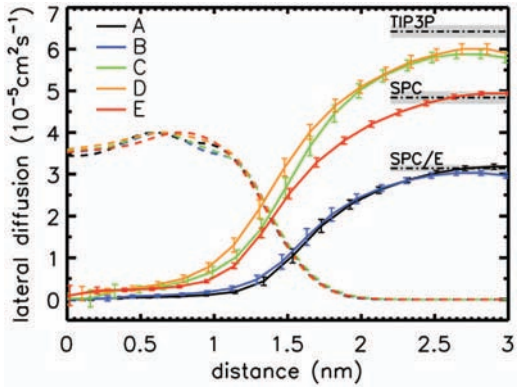

FIG. 7. (Color) The lateral diffusion coefficients of water molecules (*solid* lines) at the membrane-water interface. The *dashed* lines mark the normalized DOPC electron density profiles (superimposed at the descending slope) to indicate the location of the bilayer. The respective values for bulk water diffusion are shown as *dashed-dotted* lines (errors in *gray* shading). All diffusion coefficients (and standard errors) were measured by fitting the slope between 2 and 200 ps of the msd curves, using block averaging of length 5 ns.

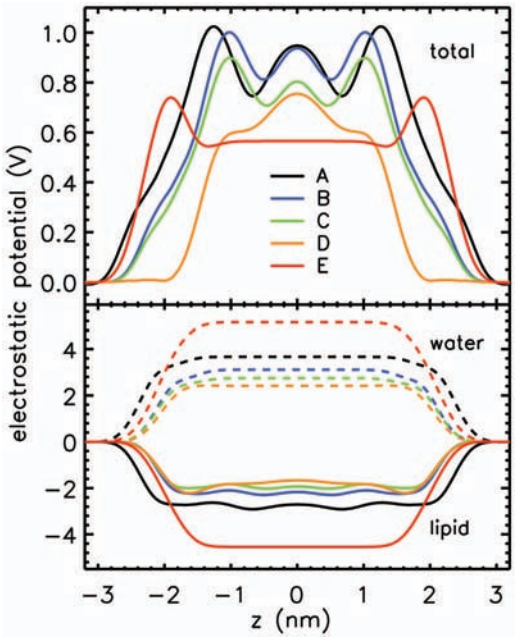

FIG. 8. (Color) Total electrostatic potential (upper panel) and contributions (lower panel) due to the lipid dipoles (*solid* lines) and due to water dipole orientation (*dashed* lines) at the membrane/water interface across the DOPC bilayer (symmetrized). The potential was averaged over the final 80 ns of the simulation.

in the interfacial region (*blue* and *black lines*, see also Lopez *et al.*,[64] both Berger-SPC and CHARMM27-TIP3P resulted in a comparingly large water diffusion of $(1-3)\times10^{-5}$ cm^2/s. This is at least partially caused by the enhanced bulk diffusion values for these water models[65] as compared to experiment (2.92×10^{-5} cm^2/s at 35 °C, see Ref. 66).

F. Electrostatic potential and dipole moment

The electrostatic potential, or the dipole potential, is known to be an important factor for the permeation of ionic species through membranes, and the insertion and proper function or regulation of membrane proteins. Lipid polar headgroups, glycerol esters, as well as water molecules were found to contribute to the total electrostatic potential, which arises from the nonrandom orientation of lipids and hydrated water in the bilayer. Experimentally, a fully saturated phospholipid was measured to have an electrostatic potential in the range of 220–280 mV.[67,68] Introducing one unsaturated segment to the acyl chains would decrease the value of the potential by as much as 30 mV.[69]

Figure 8 shows the calculated electrostatics potential of all investigated force fields. Quantitatively, all profiles are larger by a factor of 3–4 as compared to experiment. Nevertheless, they are qualitatively in agreement with experiments[70] and in accord with previous simulation studies (see, e.g., Refs. 8, 71, and 72): The potential is positive inside the bilayer, and the phospholipid headgroups contribute a negative potential (*solid* lines in Fig. 8, lower panel) which is overcompensated by the opposed water dipole orientation (*dashed* lines) in the interfacial region, resulting in a total positive electrostatic potential. The orientation of water dipoles was previously found to be reduced in the presence of salt ions.[8]

Both all-atom force fields have a distinct potential maximum at the bilayer center, caused by the nonzero partial charges on the terminal methyl groups. While the total electrostatic potential for the CHARMM27 system rises first in the region of the carbonyl groups, the potential for the GAFF system steeply increases in the choline/phosphate region (similar for both investigated water models). For the latter, the potential decreases slightly toward the unsaturated carbons of the chains followed by the central maximum. The Berger force field showed a flat potential in the region of the hydrocarbon chains which is due to the uncharged hydrocarbon tail atoms.

Besides the PC headgroup, mainly the fatty acid carbonyl groups contribute to the molecular dipole moment (see also distribution of partial charges in Table I). In crystal structures at very low hydration (two water molecules per lipid) an asymmetry between the carbonyl orientations of the *sn*-1 and *sn*-2 was observed.[73,74] The *sn*-1 carbonyl oriented parallel to the bilayer plane and the *sn*-2 carbonyl was found in two different conformations, both pointing toward the water phase (partially negatively charged oxygen pointing out of the hydrophobic core).

All force fields showed broad Gaussian-like distributions of C=O orientations with respect to the bilayer normal (data not shown). Within the Berger force field, the most probable angle ϕ between the C=O vector and the membrane normal was shifted from 60° to 31° between the *sn*-1 and *sn*-2 carbonyls, and the probabilities of finding angles below 90° (carbonyl pointing to the water phase, and carbonyl dipole toward hydrophobic core) are 86% and 97%, respectively. For GAFF (with surface tension, SPC/E water), an increase in ϕ from 54° to 69° was observed, and the probability of finding a carbonyl pointing to the water phase is 93% for the *sn*-1 and is 76% for the *sn*-2 carbonyl. The most probable carbonyl angles for the acyl chains in the CHARMM27 force field are 44° and 69°; however, the probabilities for angles $\leqslant$90° were similar for both chains with 70%.

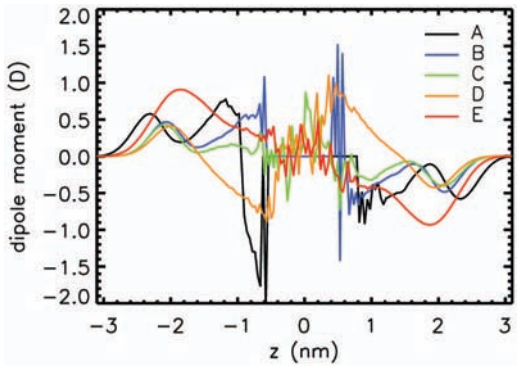

FIG. 9. (Color) Average water dipole moment along the membrane normal. The large fluctuations inside the hydrophobic core of the lipid bilayer are due to individual water molecules spontaneously permeating the membrane.

The water order in the interfacial region is further investigated in Fig. 9, showing the mean dipole moment of water molecules depending on their position relative to the lipid bilayer. Both Berger and GAFF systems revealed two regions of positive water dipole moment (pointing into the membrane, opposite to the lipid dipoles), one in the region of the choline and phosphate groups and the second at the hydrophobic interface close to the carbonyl groups. The water orientation is more pronounced for the Berger force field. This is due to the increased total dipole moment of Berger lipids (≈15% with respect to GAFF and CHARMM27) and the two times larger component of the dipole moment normal to the membrane (Table IV).

For the CHARMM27 system (D), the water dipole orientation at the interface headgroup-hydrophobic core is reversed with respect to the other force fields. Both the water model (TIP3P) and the significant amount of carbonyl dipoles pointing into the hydrophobic core (≈30%) for CHARMM27 are presumably the cause for this reversed water dipole orientation.

IV. DISCUSSION

All three investigated lipid force fields were shown to correctly describe the coarse properties of phospholipid bilayers. However, the general feature of distinctly different C2 order parameters between the two acyl chains is observed only in the newly developed GAFF for DOPC. Neither of the investigated force fields could reproduce the experimentally observed C2 splitting in the *sn*-2 chain, and indeed the two methylene hydrogen positions were found equivalent along the acyl chains in both all-atom models. The C2 splitting was suggested to be due to two different conformations of the lipid molecule or due to the magnetic inequivalence of the C2 deuterons in the NMR experiment.[51] The simulations did not provide any evidence for different C2 order parameters coupled to different lipid conformations. Possibly, a polarizable lipid force field can induce an inequivalence of the two protons due to differential shielding at the hydrophobic/hydrophilic interface.

Also the different orientations in the beginning of the two chains with respect to the bilayer normal appear to be best described by GAFF. Interestingly, Jójárt and Martinek[29] did not observe significant differences between the C2 atom orders of the palmitoyl and the oleyl chains of POPC applying GAFF. This might be due to high sensitivity of RESP charges to the conformation of the molecule (charge calculation on 12 conformations[29] versus 72 conformations here). Order parameters reported for the recently developed GROMOS96 45A3 force field for phospholipids[75] also show an enhanced order for the C2 atom of the *sn*-1 chain (DPPC). However, the latter two studies were probably based on too short sampling times (4 ns and 300 ps, respectively). A recent reparametrization of the partial charges in the CHARMM27 force field enabling simulations of the fluid phase in the *NPT* ensemble[49] did not yield improved C2 atom orders with respect to the original CHARMM27.

Both structural and dynamical properties of the aqueous solution at the water-phospholipid bilayer interface (for a thorough review on this topic see Berkowitz *et al.*[15]) were shown to depend on the phospholipid force field: The ordering of water molecules within the lipid-water interface crucially depends on the chosen lipid force field. For CHARMM27, the total electrostatic potential was shown to rise first in the region of the carbonyl groups. Together with the experimental finding that removal of the carbonyl groups only partly accounts for the positive electrostatic potential inside lipid bilayers[70] this may question the applicability of the CHARMM27 force field in cases where the potential is crucial to, e.g., the structure or function of membrane-associated proteins or in the electrostatically driven binding of molecules to membranes.

Also the water dynamics close to membrane interfaces is crucially dependent on the applied force field: CHARMM27 was developed by applying the TIP3P water model, the Berger force field together with SPC water, and GAFF may be used with both TIP3P and with SPC/E. Only the SPC/E water correctly reflects the bulk water diffusion coefficient, and TIP3P overestimates the bulk water diffusion by more than a factor of 2. For the CHARMM27 lipid bilayer simulation, the used 38 water molecules per lipid were not sufficient to reach full hydration, since the water diffusion between periodic bilayers did not reach the increased bulk water diffusion for the TIP3P water model. In contrast, for SPC and SPC/E water this hydration level was sufficient to reach the bulk water diffusion. The lateral diffusion coefficient for lipids is too small for GAFF and the Berger force field applying the SPC/E and SPC water models, respectively. In contrast, the CHARMM27 lipid force field shows a diffusion close to the experimental value. One possible reason may be due to the noteworthy charges on the acyl chain atoms in the CHARMM27 force field. Also, the diffusion is partly enhanced due to the large diffusion coefficient for water molecules applying the TIP3P model. Note that due to long-range correlations the lateral diffusion is dependent on the system size for small systems.[47] Here, due to the removal of unidirectional correlated motions the obtained results for the diffusion coefficient are likely too small.

V. SUMMARY

In the present study we show simulation results for a DOPC membrane employing a newly developed all-atom force field based on GAFF. The performance of this force field against two existing parametrizations (the all-atom CHARMM27 and the united-atom model by Berger) is tested on a range of physical observables. The presented GAFF reproduces both the coarse properties such as the bilayer thickness and also the experimentally found differences in the structure and the order of the two acyl chains. In addition, GAFF offers a consistent force field for both lipids and membrane embedded proteins, thereby enabling detailed studies of the interaction between lipids and proteins. The extension of GAFF to other phospholipids is straightforward.

It has been argued that the *NPT* ensemble is appropriate for lipid bilayer simulations.[20,76,77] Both GAFF and the CHARMM27 lipid force field showed a transition to a gel-like state in this ensemble, making the use of a surface tension mandatory in simulations of the fluid (L_α) phase. The applied surface tension in our GAFF simulations was found to be approximately independent of the size of the bilayer patch (a four times larger bilayer did not show significant changes in the area per lipid, data not shown), and should be multiplied by the number of bilayers in the simulation system. Membrane-embedded proteins will modify the membrane pressure profile in a local environment around the protein. However, for melittin embedded in a DMPC bilayer (121 lipids), even similar lateral pressures were determined for the protein-lipid system (applying CHARMM27) as compared to the pure lipid bilayer.[78] Therefore, we expect the surface tension to be only slightly affected for comparable dilute protein-lipid systems.

In the case of CHARMM27, a reparametrization of the partial atomic charges has recently been shown to pave the way toward fluid phase simulations in the *NPT* ensemble for DPPC.[49] One possible reason for deviations from the fluid-like behavior of bilayers simulated in the *NPT* ensemble applying all-atom force fields may be the neglect of polarizability. Especially the large fields occurring at the interface between the highly polar water phase and the low-dielectric hydrocarbon interior underline the need for a careful investigation of polarization effects. To this end, development and tests of a polarizable model are currently under way.

Apart from the polarization issue, future studies will focus on the lipid-protein interaction in the different force fields. However, comparison to experimental data is currently limited due to the scarcity of detailed experimental studies on these interactions. Since GAFF easily allows extension to arbitrary organic molecules it can also be applied to systematic studies on the partitioning of solutes between the solvent and the bilayer, of great importance for a more thorough understanding of dose-response relationships in medicine. Knowledge about the binding characteristics may additionally prove useful for future drug development.

ACKNOWLEDGMENTS

We thank Volkhard Helms for support with computing time and Beate Griepernau for help with the analysis. We thank Mark Abraham for providing the script for the conversion of the CHARMM27 force field to GROMACS and for a lot of helpful discussions about its use. Financial support by the Deutsche Forschungsgemeinschaft (Graduate School Structure Formation and Transport in Complex Systems, No. 1276/1) is acknowledged. As members of the Center for Bioinformatics, Rainer A. Böckmann and Shirley Siu are supported by the Deutsche Forschungsgemeinschaft Grant No. BIZ 4/1. Robert Vacha and Pavel Jungwirth thank the Grant Agency of the Academy of Sciences (Grant No. A400400503) and the Czech Ministry of Education (Grant No. LC512). R.V. acknowledges support from the Granting Agency of the Czech Republic (Grant No. 203/05/H001).

PDB files of equilibrated snapshots, and the GROMACS implementations of the used Berger and CHARMM27 force field as well as that of the developed GAFF for DOPC molecules are available free of charge on the websites http://www.bioinf.uni-sb.de/RB and http://www.molecular.cz/~vacha/downloade.htm.

[1] J. R. Trudell, Anesthesiology **46**, 5 (1977).
[2] R. S. Cantor, Biochemistry **36**, 2339 (1997).
[3] J. R. Silvius, Biochim. Biophys. Acta **1610**, 174 (2003).
[4] C. Hofsäß, E. Lindahl, and O. Edholm, Biophys. J. **84**, 2192 (2003).
[5] B. W. Urban, Pharmacol. Ther. **111**, 729 (2006).
[6] C.-J. Högberg and A. P. Lyubartsev, Biophys. J. **94**, 525 (2008).
[7] S. A. Pandit, D. Bostick, and M. L. Berkowitz, Biophys. J. **84**, 3743 (2003).
[8] R. A. Böckmann, A. Hac, T. Heimburg, and H. Grubmüller, Biophys. J. **85**, 1647 (2003).
[9] L. Herbette, C. A. Napolitano, and R. V. McDaniel, Biophys. J. **46**, 677 (1984).
[10] R. A. Böckmann and H. Grubmüller, Angew. Chem., Int. Ed. **43**, 1021 (2004).
[11] T. Heimburg and A. D. Jackson, Proc. Natl. Acad. Sci. U.S.A. **102**, 9790 (2005).
[12] T. Heimburg and A. D. Jackson, Biophys. J. **92**, 3159 (2007).
[13] D. P. Tieleman, S. J. Marrink, and H. J. C. Berendsen, Biochim. Biophys. Acta **1331**, 235 (1997).
[14] W. L. Ash, M. R. Zlomislic, E. O. Oloo, and D. P. Tieleman, Biochim. Biophys. Acta **1666**, 158 (2004).
[15] M. L. Berkowitz, D. L. Bostick, and S. Pandit, Chem. Rev. (Washington, D.C.) **106**, 1527 (2006).
[16] F. Castro-Roman, R. W. Benz, S. H. White, and D. J. Tobias, J. Phys. Chem. B **110**, 24157 (2006).
[17] S. E. Feller and J. A. D. MacKerell, J. Phys. Chem. B **104**, 7510 (2000).
[18] M. Schlenkrich, J. Brickmann, A. D. MacKerell, and M. Karplus, *Empirical Potential Energy Function for Phospholipids: Criteria for Parameter Optimization and Applications* (Birkhäuser, Boston, 1996), pp. 31–81.
[19] S.-W. Chiu, M. Clark, V. Balaji, S. Subramaniam, H. L. Scott, and E. Jakobsson, Biophys. J. **69**, 1230 (1995).
[20] O. Berger, O. Edholm, and F. Jähnig, Biophys. J. **72**, 2002 (1997).
[21] W. L. Jorgensen and J. Tirado-Rives, J. Am. Chem. Soc. **110**, 1657 (1988).
[22] D. P. Tieleman, J. L. MacCallum, W. L. Ash, C. Kandt, Z. Xu, and L. Monticelli, J. Phys.: Condens. Matter **18**, S1221 (2006).
[23] G. Kaminski, R. A. Friesner, J. Tirado-Rives, and W. L. Jorgensen, J. Phys. Chem. B **105**, 6474 (2001).
[24] S. W. I. Siu and R. A. Böckmann, J. Struct. Biol. **157**, 545 (2007).
[25] B. Griepernau, S. Leis, M. F. Schneider, M. Sikor, D. Steppich, and R. A. Böckmann, Biochim. Biophys. Acta **1768**, 2899 (2007).
[26] M. Patra, E. Salonen, E. Terama, I. Vattulainen, R. Faller, B. W. Lee, J. Holopainen, and M. Karttunen, Biophys. J. **90**, 1121 (2006).
[27] J. Chanda and S. Bandyopadhyay, Langmuir **22**, 3775 (2006).
[28] J. Wang, R. M. Wolf, J. W. Caldwell, P. A. Kollman, and D. A. Case, J. Comput. Chem. **25**, 1157 (2004).
[29] B. Jójárt and T. A. Martinek, J. Comput. Chem. **28**, 2051 (2007).
[30] C. I. Bayly, P. Cieplak, W. D. Cornell, and P. A. Kollman, J. Phys. Chem. **97**, 10269 (1993).

[31] W. D. Cornell, P. Cieplak, C. I. Bayly, and P. A. Kollman, J. Am. Chem. Soc. **115**, 9620 (1993).
[32] S. E. Feller, D. Yin, R. W. Pastor, and A. D. MacKerell, Biophys. J. **73**, 2269 (1997).
[33] http://persweb.wabash.edu/facstaff/fellers.
[34] S. Tristram-Nagle, H. I. Petrache, and J. F. Nagle, Biophys. J. **75**, 917 (1998).
[35] W. F. van Gunsteren and H. J. C. Berendsen, Gromos User Manual, BIOMOS biomolecular software, Laboratory of Physical Chemistry, University of Groningen, The Netherlands, 1987.
[36] M. J. Frisch, G. W. Trucks, H. B. Schlegel *et al.*, GAUSSIAN 03, Revision C.02, Gaussian, Inc., Wallingford, CT, 2004.
[37] H. J. C. Berendsen, J. P. M. Postma, W. F. van Gunsteren, and J. Hermans, *Interaction Model for Water in Relation to Protein Hydration* (Reidel, Dordrecht, The Netherlands, 1981), pp. 331–342.
[38] W. L. Jorgensen, J. Chandrasekhar, and J. D. Madura, J. Chem. Phys. **79**, 926 (1983).
[39] H. J. C. Berendsen, J. R. Grigera, and T. P. Straatsma, J. Phys. Chem. **91**, 6269 (1987).
[40] H. J. C. Berendsen, D. van der Spoel, and R. van Drunen, Comput. Phys. Commun. **91**, 43 (1995).
[41] E. Lindahl, B. Hess, and D. van der Spoel, J. Mol. Model. **7**, 306 (2001).
[42] H. J. C. Berendsen, J. P. M. Postma, W. F. van Gunsteren, A. Dinola, and J. R. Haak, J. Chem. Phys. **81**, 3684 (1984).
[43] B. Hess, H. Bekker, H. J. C. Berendsen, and J. G. E. M. Fraaije, J. Comput. Chem. **18**, 1463 (1997).
[44] S. Miyamoto and P. A. Kollman, J. Comput. Chem. **13**, 952 (1992).
[45] J. Seelig, Q. Rev. Biophys. **10**, 353 (1977).
[46] J. P. Douliez, A. Ferrarini, and E. J. Dufourc, J. Chem. Phys. **109**, 2513 (1998).
[47] J. B. Klauda, B. R. Brooks, and R. W. Pastor, J. Chem. Phys. **125**, 144710 (2006).
[48] M. O. Jensen, O. G. Mouritsen, and G. H. Peters, Biophys. J. **86**, 3556 (2004).
[49] J. Sonne, M. O. Jensen, F. Y. Hansen, L. Hemmingsen, and G. H. Peters, Biophys. J. **92**, 4157 (2007).
[50] R. W. Benz, F. Castro-Roman, D. J. Tobias, and S. H. White, Biophys. J. **88**, 805 (2005).
[51] J. Seelig and N. Waespe-Sarcevio, Biochemistry **17**, 3310 (1978).
[52] S. A. Pandit, S.-W. Chiu, E. Jakobsson, A. Grama, and H. L. Scott, Biophys. J. **92**, 920 (2007).
[53] D. E. Warschawski and P. F. Devaux, Eur. Biophys. J. **34**, 987 (2005).
[54] A. Seelig and J. Seelig, Biochim. Biophys. Acta **406**, 1 (1975).
[55] P. B. Hitchcock, R. Mason, K. M. Thomas, and G. G. Shipley, Proc. Natl. Acad. Sci. U.S.A. **71**, 3036 (1974).
[56] J. B. Klauda, B. R. Brooks, A. D. MacKerell, R. M. Venable, and R. W. Pastor, J. Phys. Chem. B **109**, 5300 (2005).
[57] S. Y. Bhide and M. L. Berkowitz, J. Chem. Phys. **123**, 224702 (2005).
[58] S. W. Chiu, E. Jakobsson, S. Subramaniam, and H. L. Scott, Biophys. J. **77**, 2462 (1999).
[59] A. K. Engel and D. Cowburn, FEBS Lett. **126**, 169 (1981).
[60] S. König, T. M. Bayerl, G. Coddens, D. Richter, and E. Sackmann, Biophys. J. **68**, 1871 (1995).
[61] A. Filippov, G. Orädd, and G. Lindblom, Langmuir **19**, 6397 (2003).
[62] W. Pfeiffer, T. Henkel, E. Sackmann, and W. Knoll, Europhys. Lett. **8**, 201 (1989).
[63] J. Tabony and B. Perly, Biochim. Biophys. Acta **1063**, 67 (1990).
[64] C. F. Lopez, S. O. Nielsen, and M. L. Klein, J. Phys. Chem. B **108**, 6603 (2004).
[65] M. W. Mahoney and W. L. Jorgensen, J. Chem. Phys. **114**, 363 (2001).
[66] R. Mills, J. Phys. Chem. **77**, 685 (1973).
[67] H. Brockman, Chem. Phys. Lipids **73**, 57 (1994).
[68] R. J. Clarke, Adv. Colloid Interface Sci. **89**, 263 (2001).
[69] R. J. Clarke, Biochim. Biophys. Acta **1327**, 269 (1997).
[70] K. Gawrisch, D. Ruston, J. Zimmerberg, V. A. Parsegian, R. P. Rand, and N. Fuller, Biophys. J. **61**, 1213 (1992).
[71] R. J. Mashl, H. L. Scott, S. Subramaniam, and E. Jacosson, Biophys. J. **81**, 3005 (2001).
[72] A. A. Pandit, D. Bostick, and M. L. Berkowitz, J. Chem. Phys. **119**, 2199 (2003).
[73] R. H. Pearson and I. Pascher, Nature (London) **281**, 499 (1979).
[74] H. Hauser, I. Pascher, R. H. Pearson, and S. Sundell, Biochim. Biophys. Acta **650**, 21 (1981).
[75] I. Chandrasekhar, M. Kastenholz, R. D. Lins, C. Oostenbrink, L. D. Schuler, D. P. Tieleman, and W. F. van Gunsteren, Eur. Biophys. J. **32**, 67 (2003).
[76] F. Jähnig, Biophys. J. **71**, 1348 (1996).
[77] S. J. Marrink and A. E. Mark, J. Phys. Chem. **105**, 6122 (2001).
[78] J. Gullingsrud, A. Babakhani, and J. A. McCammon, Mol. Simul. **32**, 831 (2006).
[79] Y. Liu and J. F. Nagle, Phys. Rev. E **69**, 040901 (2004).